

## Polarization properties of single zinc-blende GaN/AlN quantum dots

S. Sergent,<sup>1</sup> S. Kako,<sup>2</sup> M. Bürger,<sup>3</sup> T. Schupp,<sup>3</sup> D. J. As,<sup>3</sup> and Y. Arakawa<sup>1,2</sup>

<sup>1</sup>*Institute for Nano Quantum Information Electronics, The University of Tokyo, 4-6-1 Komaba, Meguro, Tokyo 153-8505, Japan*

<sup>2</sup>*Institute of Industrial Science, The University of Tokyo, 4-6-1 Komaba, Meguro, Tokyo 153-8505, Japan*

<sup>3</sup>*Universität Paderborn, Department Physik, 33095 Paderborn, Germany*

(Received 2 June 2014; revised manuscript received 14 October 2014; published 18 December 2014)

We study by microphotoluminescence the polarization properties of single zinc-blende GaN/AlN quantum dots fabricated by two growth processes: the droplet epitaxy technique and the Stranski-Krastanov growth mode. A statistical analysis of their polarization properties both at the mesoscopic and nanoscopic scales indicates that it is possible to modify the phase and amplitude of their valence band mixing by switching on and off the influence of AlN antiphase domains through the growth process.  $k \cdot p$  calculations show that the strain effects and quantum dot geometries resulting from the growth process play a major role in shaping their polarization properties.

DOI: [10.1103/PhysRevB.90.235312](https://doi.org/10.1103/PhysRevB.90.235312)

PACS number(s): 78.55.Cr, 78.67.Hc, 81.07.Ta

### I. INTRODUCTION

Due to a large exciton-binding energy and large band offsets, GaN quantum dots (QDs) are attractive solid state emitters for optoelectronic devices operating at high temperature, such as nanolasers, single photon sources, and quantum information devices. For instance, single-photon emission has been observed up to 200 K in self-assembled wurtzite GaN QDs [1] and even up to 300 K in site-controlled nanowire QDs [2]. Zinc-blende (ZB) GaN QDs are less studied [3–7] than their wurtzite counterparts because the ZB phase of group-III nitrides is metastable, so that high-quality epilayers are difficult to obtain. However, ZB GaN QDs present many advantages over self-assembled wurtzite GaN QDs such as shorter radiative lifetimes and larger oscillator strengths [3,5], a reduced spectral diffusion [5], and a better photon antibunching at low temperature [ $g^2(0) = 0.25$ ] [6]. In addition, the single-photon emission of ZB GaN QDs has already been observed up to 100 K, thus proving their potential for high-temperature operation [6]. The polarization properties of ZB GaN QDs are still little known since a single study has been carried out on the macroscopic polarization properties of a QD ensemble by Lagarde *et al.* who reported on the optical orientation of the exciton spin at room temperature [7]. A good understanding of the polarization properties of individual ZB GaN QDs is, however, essential to access their excitonic states [8], to estimate and tailor the phase and amplitude of valence band mixing [9–12] or the fine-structure splitting [13–15] and to assess their potential for quantum information devices [16].

The growth of ZB GaN QDs has been originally demonstrated by plasma-assisted molecular beam epitaxy in the frame of the Stranski-Krastanov (SK) growth mode [17]. More recently, a droplet epitaxy (DE) technique has also been developed and allows for greater control of the QD structural properties, especially their density [18]. Because the valence band mixing of QDs is strongly affected by their morphology or their strain distribution, the growth process has a major impact on their polarization properties and one would expect significant differences between DE QDs and SK QDs.

In this paper, we report on the polarization-dependent microphotoluminescence ( $\mu$ PL) of self-assembled ZB GaN QDs grown either in the frame of the SK mode or by the

DE technique. As opposed to the previous macropolarization report by Lagarde *et al.* [7], the study of their polarization properties both at the mesoscopic and nanoscopic scales shows that SK QDs present a significant amount of valence band mixing and that it is possible to influence the valence band mixing of ZB GaN QDs through the growth process. Additional  $k \cdot p$  calculations show us that the stark difference between DE and SK QDs arises from the larger inplane anisotropy induced by the strain-based SK growth mode.

The paper is organized as follows. In order to facilitate the discussion in the following sections, we introduce in Sec. II the basics of the valence band mixing in self-assembled QDs and we investigate by  $k \cdot p$  calculations the influence of shape and stress anisotropy on ZB GaN QDs. Section III describes the fabrication process of the samples, their basic structural and optical properties, and the experimental setup used to study the polarization properties of ZB GaN QDs. In Sec. IV, we study by  $\mu$ PL the polarization properties of both SK and DE ZB GaN QD ensembles on a mesoscopic scale and we evidence that only SK ensembles are strongly influenced by the presence of antiphase domains (APDs). In Sec. V, we perform a statistical analysis of the polarization properties of individual ZB GaN QDs grown by the DE and the SK processes. We show that SK QDs present a significant valence band mixing and that they tend to be polarized along [110] or  $[1\bar{1}0]$  depending on the APD they are located in. On the opposite, we find that the polarization orientation of individual DE QDs is not significantly influenced by the APDs and they present on average a lower amount of valence band mixing. Experimental results are then discussed in Sec. VI in light of the  $k \cdot p$  calculations performed in Sec. II. We finally conclude in Sec. VII.

### II. VALENCE BAND MIXING

In an ideal QD with a high  $C_{\infty v}$  symmetry, the neutral bright exciton can be described as two energy-degenerated circularly polarized states  $|J\rangle = |\pm 1\rangle$  with  $J$  the total angular momentum. Self-assembled ZB QDs grown on the (001) plane usually have a lower  $C_{2v}$  symmetry so that the neutral exciton actually consists of two eigenstates  $|X\rangle$  and  $|Y\rangle$  that are linear combinations of  $|\pm 1\rangle$ .  $|X\rangle$  and  $|Y\rangle$  are linearly polarized along the main crystallographic axes of the QD plane [110] and  $[1\bar{1}0]$

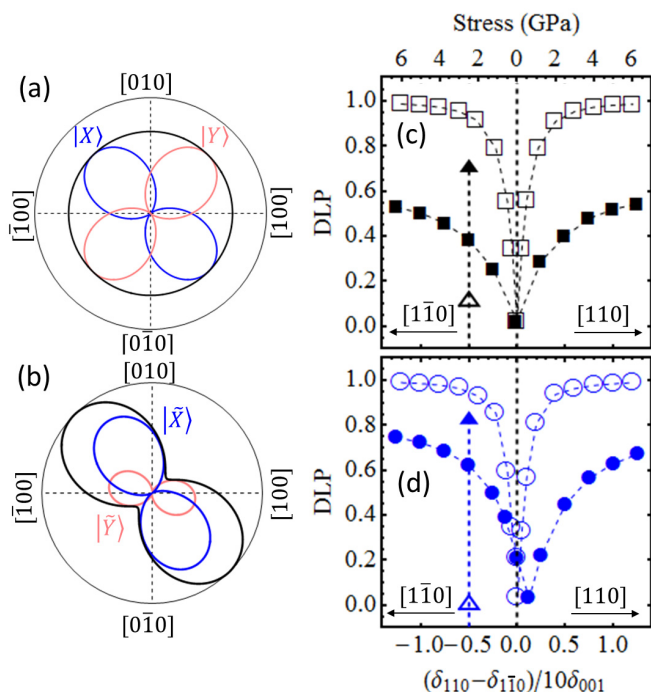


FIG. 1. (Color online) Representation of the QD polarization properties: (a) without valence band mixing and (b) with valence band mixing as calculated for a lens-shape ZB GaN QD with height  $\delta_{001} = 2.5$  nm,  $\sigma = 0$  and inplane aspect parameter  $\alpha = (\delta_{110} - \delta_{1\bar{1}0})/10\delta_{001} = -0.75$  ( $\delta_{110}$  and  $\delta_{1\bar{1}0}$  are the dimensions of the QD along  $[110]$  and  $[1\bar{1}0]$ ). The resulting DLP is 69%. The blue and pink lines correspond, respectively, to eigenstates  $|X\rangle$  and  $|Y\rangle$  or  $|\tilde{X}\rangle$  and  $|\tilde{Y}\rangle$ . The black line corresponds to the total QD polarization. (c) DLP of truncated-pyramid SK QDs for various  $\alpha$  (closed squares) and  $\sigma$  (open squares). (d) Same as (c) for lens-shape DE QDs. Lines are guides for the eye. Arrows indicate the orientation of stress and shape anisotropy. The closed (open) triangles represent the DLP calculated for QDs with  $\alpha = \pm 0.5$  and  $\sigma = 0.5$  GPa applied along  $[1\bar{1}0]$ .

[see Fig. 1(a)] and are generally split in energy by the so-called fine-structure splitting due to the electron-hole exchange interaction [10, 14, 19]. In the absence of valence band mixing and under nonresonant weak excitation, both eigenstates exhibit the same intensity [8]. However, the morphology, the strain distribution, or the piezoelectric field of fabricated QDs usually present inplane anisotropies that further lower the QD symmetry and lead to a valence band mixing between heavy hole (HH) and lower valence band states [light hole (LH) band and spin-orbit split-off (SO) band]. As a result of this valence band mixing, the new  $|\tilde{X}\rangle$  and  $|\tilde{Y}\rangle$  eigenstates are not necessarily orthogonally cross-polarized, their radiative recombination rates  $\gamma_x$  and  $\gamma_y$  can be different and, providing that an efficient additional relaxation channel exists [8], their intensities under weak nonresonant excitation may differ significantly because they do not only depend on the QD pumping rate anymore. The total QD intensity thus presents a nonzero degree of linear polarization  $DLP = \frac{I_{\min} - I_{\max}}{I_{\min} + I_{\max}}$  [Fig. 1(b)]. To quantify the relation between inplane anisotropy and DLP, we perform  $k \cdot p$  calculations of ZB GaN/AlN QDs (see details in the Appendix) for QDs elongated along  $[110]$  and  $[1\bar{1}0]$

[Figs. 1(c) and 1(d)]. DLPs as high as 53% (respectively, 80%) are found for truncated pyramid SK QDs (respectively, lens-shape DE QDs) in a range of inplane anisotropies that are consistent with structural data [18]. When the calculations are performed for various applied stresses  $\sigma$ , one can observe that a DLP larger than 90% can be obtained for values larger than 2 GPa [Figs. 1(c) and 1(d)]. As confirmed by the calculation of valence bands contributions to the hole states, such large DLPs emerge from the mixing of the HH band with both the LH and SO bands (see Appendix). Let us note that the QD behavior is not symmetric in the  $[110]$  and  $[1\bar{1}0]$  directions and that the valence band mixing of symmetric dots with  $\sigma = 0$  is nonzero: DLPs of 2% and 21% are found for SK QDs and DE QDs, respectively. This is mainly due to the symmetry reduction induced by the presence of the piezoelectric field, as calculations excluding the piezoelectric field lead to  $DLP < 0.002\%$ . Such an asymmetric behavior has already been found in ZB InAs QDs [19], but the DLPs calculated here are significantly larger: this is first due to the inclusion of the piezoelectric field in the calculation and second, to the smaller spin-orbit split-off energy in ZB GaN [20].

As we will show experimentally in Sec. V, we should mention that the  $|\tilde{X}\rangle$  and  $|\tilde{Y}\rangle$  eigenstates are not always observable when probing the excitonic transitions of a single QD in the (001) plane under weak nonresonant excitation. This is especially true in three cases:

- (i) the observed line is a charged exciton, so that no cross-polarized state exists (see, e.g., Ref. [12]),
- (ii) the observed line is a neutral exciton but the fine-structure splitting between the two cross-polarized states is smaller than the QD broadening, so that they cannot be distinguished (see, e.g., Refs. [8, 16]),
- (iii) the observed line is a neutral exciton with a fine structure splitting larger than the QD broadening but due to valence band mixing, the intensity of the cross-polarized state is too low to be observable.

In cases (i) and (ii), the QD thus has a DLP equal to 0 providing that there is no valence band mixing and a DLP larger than 0 if there is some valence band mixing [see black lines in Figs. 1(a) and 1(b)]. In case (iii), the observed emission peak has a complete linear polarization, i.e., a DLP equal to 1. The latter case is typically what one would expect for large external stresses  $\sigma$  [open symbols in Figs. 1(c) and 1(d)] or when both the effects of inplane aspect ratio and external stress compound to lead to large amplitude of valence band mixing [closed triangles in Figs. 1(c) and 1(d)].

### III. SAMPLE AND EXPERIMENTAL SETUP

The self-assembled ZB GaN/AlN QDs studied in this paper are grown by plasma-assisted molecular beam epitaxy in the SK mode [21] or by the DE technique [22] on 3C-SiC/Si (001) pseudosubstrates. The sample substrates are constituted of a 10- $\mu\text{m}$  3C-SiC(001) layer deposited by low-pressure chemical vapor deposition on a 500- $\mu\text{m}$  Si (001) substrate. From the atomic force microscopy (AFM) scans of uncapped QDs, we estimate the QD density to be larger than  $10^{11} \text{ cm}^{-2}$  for SK QDs and  $10^{10} \text{ cm}^{-2}$  for DE QDs. Because of the high-density of QDs obtained by the two growth processes, submicrometer mesas are processed in some areas of the samples by electron

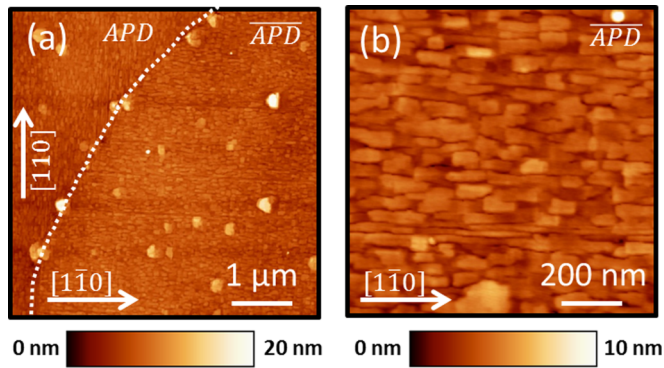


FIG. 2. (Color online) (a)  $5 \times 5\text{-}\mu\text{m}$  AFM scan of the top AlN surface evidencing the presence of two antiphase domains. The dashed line highlights the domain boundary. Orthogonal domains oriented along  $[110]$  and  $[1\bar{1}0]$  are labeled APD and  $\overline{\text{APD}}$ , respectively. (b)  $1 \times 1\text{-}\mu\text{m}$  AFM scan of the top AlN surface for  $\overline{\text{APD}}$ .

beam lithography of a spin-coated resist and subsequent  $\text{Cl}_2/\text{Ar}$  ion-coupled plasma reactive ion etching of the epilayer. This allows us to reduce the amount of QDs probed by the  $\mu\text{PL}$  setup and facilitates the observation of single QDs. AFM scans of the top AlN surface of samples prior to mesa patterning reveal two types of antiphase domains extending over several hundreds of square micrometers [Figs. 2(a) and 2(b)]. For each type of domain, named, respectively, APD and  $\overline{\text{APD}}$ , AlN grains are elongated along the  $[110]$  and along the  $[1\bar{1}0]$  directions. As already reported for bulk ZB GaN epilayers grown on 3C-SiC/Si(001) [23], the grain orientation follows preferential growth axes determined by  $90^\circ$ -rotated antiphase domains in the 3C-SiC grown on Si (001) where either the C-terminated or the Si-terminated  $\{111\}$  planes spontaneously align with the  $\{111\}$  planes of Si [24].

To investigate their polarization properties, the QD samples are placed in a He-cooled cryostat at  $T = 4$  K, excited nonresonantly in grazing incidence geometry by a frequency-quadrupled continuous-wave (CW) laser emitting at 266 nm. The  $\mu\text{PL}$  signal is collected by a microscope objective (numerical aperture 0.4) that is normal to the sample surface, i.e., aligned along the  $[001]$  direction. Then the QD  $\mu\text{PL}$  signal is spatially filtered by a pinhole, dispersed on 300, 1200, or 2400 grooves/mm gratings, and collected by a nitrogen-cooled charge-coupled device camera. The spectral resolution of the setup can be as good as  $100 \mu\text{eV}$ . In order to bypass the spectrometer polarization response function, the signal polarization is analyzed by a half-wave plate followed by a Glan-Taylor linear polarizer placed just after the microscope objective.  $\theta$  is the transmission angle of this polarization analyzer in the  $(001)$  plane and it is oriented so that a  $\theta = 0^\circ$  (respectively,  $90^\circ$ ) polarization angle correspond to the  $[100]$  (respectively,  $[010]$ ) direction. For the measurements described hereafter, control experiments have been conducted to confirm that the polarization of the excitation source does not influence the measured polarization properties of ZB GaN QDs. We analyze the QD polarization by fitting the integrated luminescence intensity  $I$  with a function of the form  $I(\theta) = I_{\max} \cdot \cos^2(\theta - \theta_0) + I_{\min} \cdot \sin^2(\theta - \theta_0)$ .

The  $\mu\text{PL}$  spectra of the SK QD ensembles measured in APD and  $\overline{\text{APD}}$  domains both present a Gaussian distribution

centered at 3.5 eV with a 220 meV full-width at half-maximum. Well-isolated individual peaks can be observed on the high-energy side of the Gaussian distribution of the ensemble  $\mu\text{PL}$  signal, similar to Ref. [5]. Polarization measurements are carried out on 38 different single SK QDs emitting at energies ranging from 3.5 to 4.06 eV and located in both types of antiphase domain. The  $\mu\text{PL}$  spectra of the DE QD ensemble present a distribution centered at 3.6 eV with a 400-meV full-width at half-maximum. Because of the lower QD density obtained by the DE technique, individual QD peaks can be observed on almost all processed mesas, similar to [25], thus facilitating the collection of a significant data sample. Polarization measurements are carried out on 61 different single DE QDs emitting at energies ranging from 3.56 to 4.25 eV.

#### IV. MESOSCOPIC POLARIZATION

The two-dimensional mapping of the SK QD  $\mu\text{PL}$  integrated intensity for transmission angles of a polarization analyzer  $\theta = 45^\circ$  (i.e., along  $[110]$ ) and  $\theta = -45^\circ$  (i.e., along  $[1\bar{1}0]$ ) exhibit complementary patterns. They evidence the presence of cross-polarized domains that we, respectively, associate to APD and  $\overline{\text{APD}}$  [Figs. 3(a) and 3(b)]. The  $\overline{\text{APD}}$  SK QD ensemble turns out to be polarized along  $[1\bar{1}0]$  ( $\theta_0 = -45^\circ$ ) and to present a large degree of linear polarization DLP = 74% [black dots in Fig. 3(c)]. Such a large DLP

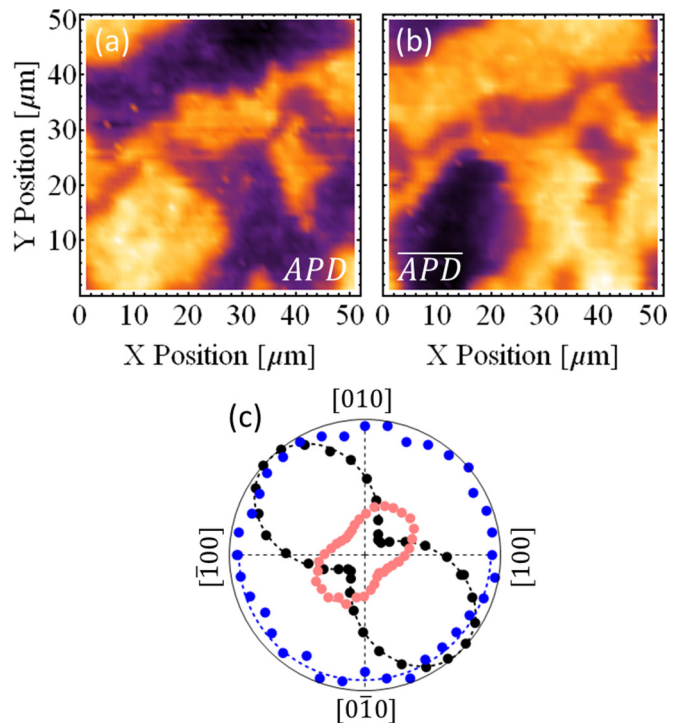


FIG. 3. (Color online) Two-dimensional map of the SK QD  $\mu\text{PL}$  integrated intensity in a given area of the sample for transmission angles of the polarization analyzer (a)  $\theta = 45^\circ$  and (b)  $\theta = -45^\circ$  highlighting, respectively, APD and  $\overline{\text{APD}}$  domains. (c) Polar plot of the integrated intensity of QD ensembles as a function of  $\theta$  for a DE QD ensemble (blue dots) and SK QD ensembles located in APD (pink dots) and  $\overline{\text{APD}}$  (black dots). The dashed lines are fitting curves of the form  $I(\theta) = I_{\max} \cdot \cos^2(\theta - \theta_0) + I_{\min} \cdot \sin^2(\theta - \theta_0)$ . For each sample the intensity is normalized to the maximum intensity.

shows that individual  $\overline{\text{APD}}$  SK QDs have a significant DLP as well as a preferential orientation. They thus present some valence band mixing due to in-plane anisotropies. The APD SK QD ensemble is cross-polarized in the  $[110]$  direction ( $\theta_0 = -45^\circ$ ) [pink dots in Fig. 3(c)]. It presents a smaller degree of linear polarization  $\text{DLP} = 39\%$ , which suggests either a smaller degree of QD anisotropy or a more randomly distributed polarization angle for individual QDs. This issue will be addressed in Sec. V. As the QD density is constant for all domains, the lower intensity of the APD SK QD ensemble [pink dots in Fig. 3(c)] evidences a higher degree of crystal disorder leading to a higher number of nonradiative recombination centers. This is consistent with what has been reported for bulk GaN epilayers where the crystalline quality depends on the antiphase domain orientation and where a higher level of defects (stacking faults and wurtzite phase inclusions) has been found in APD domains [23].

As opposed to SK QDs, two-dimensional mapping of the DE QD  $\mu\text{PL}$  for transmission angles of the polarization analyzer  $\theta = 45^\circ$  and  $\theta = -45^\circ$  does not highlight the presence of antiphase domains. Actually, DE QD mesoscopic ensembles tend to be unpolarized as depicted in Fig. 3(c). This readily shows that the strain distribution and the morphology of DE QDs are not affected by the presence of antiphase domains.

## V. SINGLE QUANTUM DOT POLARIZATION

### A. Stranski-Krastanov quantum dots

When we turn to individual SK QDs, we actually observe QD emission lines presenting DLPs always larger than 95% with a suppression of the QD intensity down to noise level (Fig. 4). As opposed to other semiconductor QDs [8–15,26], a second cross-polarized excitonic line is never observable within a spectral range of a few meV, despite the fact that the fine structure splitting of ZB GaN QDs has been calculated to be within this range [27]. The absence of a second cross-polarized line can be explained by cases (i), (ii), and (iii) described earlier. In any of those cases, the large measured DLPs evidence that the amplitude of valence band mixing in such single SK QDs is even larger than could be inferred from the QD ensemble polarization measurements. Because the DLP of all the observed single SK QDs is very large, the smaller DLP of the APD and  $\overline{\text{APD}}$  SK QD ensembles actually reflects the distribution of the polarization orientation of individual QDs. This is confirmed by the statistics of polarization angles displayed in Fig. 4(d). It shows that single SK QDs located in  $\overline{\text{APD}}$  domains [black bars in Fig. 4(d)] can have various orientations ranging between  $-80^\circ$  and  $70^\circ$  but that they are more likely to be polarized close to the  $[1\bar{1}0]$  direction. Conversely, APD single SK QDs [pink bars in Fig. 4(d)] tend to be polarized closer to the  $[110]$  direction, although the trend is less pronounced than for  $\overline{\text{APD}}$ , as could be inferred from the smaller DLP of the APD mesoscopic ensemble [Fig. 3(c)].

### B. Droplet epitaxy quantum dots

As opposed to SK QDs, most of the single DE QDs present a DLP larger than 70% (Fig. 5) but rarely exhibit an extinction of the QD line intensity down to noise level. In addition, individual DE QDs can present a DLP as small as

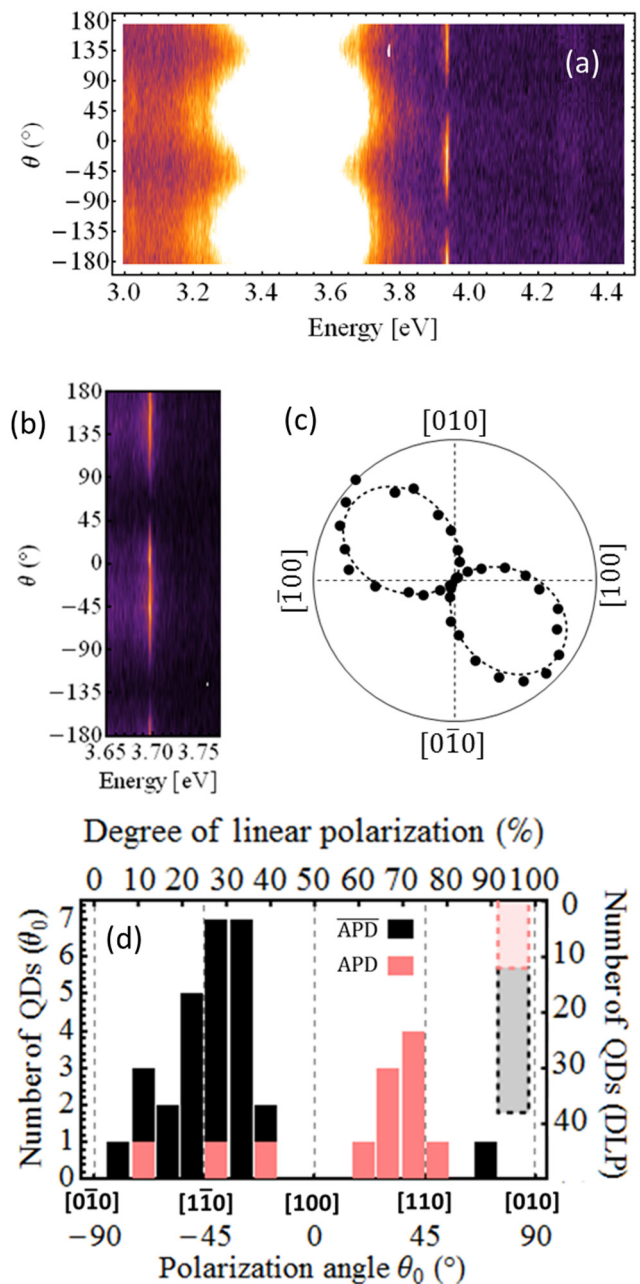


FIG. 4. (Color online) (a)  $\mu\text{PL}$  spectrum of an APD SK QD mesa for various transmission angles  $\theta$  of the polarization analyzer depicting the QD ensemble luminescence and one spectrally isolated single QD peak at 3.93 eV. (b)  $\theta$ -dependent  $\mu\text{PL}$  spectra of a single SK QD emitting at 3.70 eV and emerging from a different mesa. (c) Polar plot of the integrated intensity of the single SK QD displayed in (b). The dashed line is a fitting curve of the form  $I(\theta) = I_{\max} \cdot \cos^2(\theta - \theta_0) + I_{\min} \cdot \sin^2(\theta - \theta_0)$ . The measured QD DLP is 98% and the polarization angle is  $\theta_0 = -37^\circ$ . (d) Statistics of the polarization angle (bottom-left axes) and the degree of linear polarization (top-right axes) of 38 single SK QDs found in both APD (pink bars) and  $\overline{\text{APD}}$  (black bars) domains. For all SK QDs, the degree of linear polarization is larger than 95%.

12% [Fig. 6(a)]. This evidences a lower valence band mixing of DE QDs as compared to SK QDs and shows that the DE technique enables the growth of ZB GaN QDs presenting lower

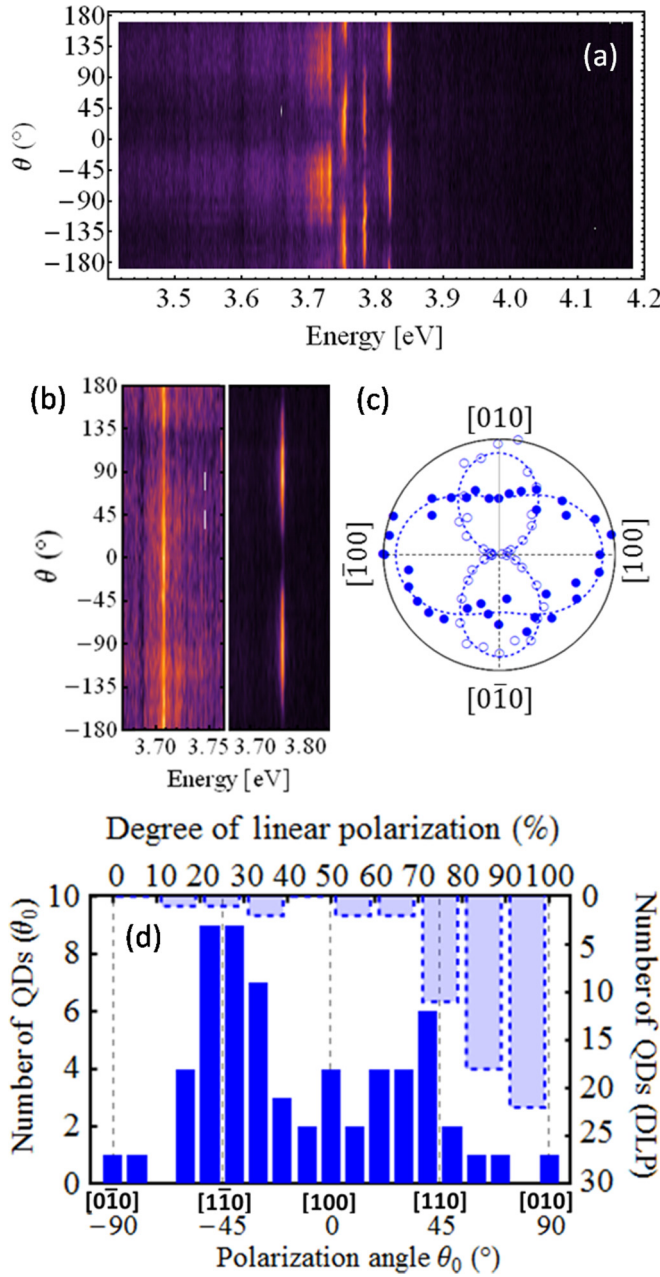


FIG. 5. (Color online) (a)  $\mu$ PL spectrum of a DE QD mesa for various transmission angles  $\theta$  of the polarization analyzer depicting spectrally isolated single QD peaks at 3.76, 3.78, and 3.82 eV. (b)  $\theta$ -dependent  $\mu$ PL spectra of single DE QDs emitting at 3.71 and 3.77 eV and emerging from two different mesas. (c) Polar plot of the integrated intensity of the QDs displayed in (b) (respectively, closed and open circles). The dashed line is a fitting curve of the form  $I(\theta) = I_{\max} \cdot \cos^2(\theta - \theta_0) + I_{\min} \cdot \sin^2(\theta - \theta_0)$ . The QD DLP is, respectively, 28% and 91% and the polarization angle is, respectively,  $\theta_0 = 3^\circ$  and  $\theta_0 = 90^\circ$ . (d) Statistics of the polarization angle (bottom-left axes) and the degree of linear polarization (top-right axes) of 61 single DE QDs.

inplane anisotropy. None of the DE QDs studied here allows us to observe the exciton fine structure splitting. Because the DE QD linear polarization is not complete, the explanations for this behavior can be reduced to cases (i) and (ii) mentioned earlier. Let us note that the latter case is consistent with the lower end

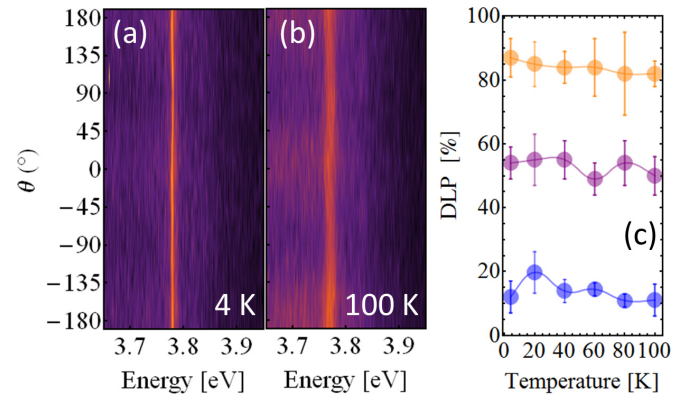


FIG. 6. (Color online)  $\mu$ PL spectra of a single DE QD for various transmission angles  $\theta$  of the polarization analyzer at (a) 4 K with DLP =  $12 \pm 5\%$ , and (b) 100 K with DLP =  $11 \pm 5\%$ . (c) DLP of three different DE QDs as a function of temperature. The lowest DLP data correspond to the QD observed in Figs. 6(a) and 6(b). Lines are guides for the eye. Vertical bars represent the error on the  $I(\theta) = I_{\max} \cdot \cos^2(\theta - \theta_0) + I_{\min} \cdot \sin^2(\theta - \theta_0)$  fitting.

(a few hundreds of  $\mu$ eV) of the fine structure-splitting range calculated for ZB GaN QDs [27]. Finally, as could be inferred from the mesoscopic polarization properties, the polarization orientation of single DE QDs is more randomly distributed than for SK QDs [Fig. 5(d)]. Nevertheless, DE QDs tend to be oriented along the two orthogonal crystallographic axes [110] and  $[1\bar{1}0]$ , which is still consistent with an unpolarized DE QD ensemble [Fig. 3(c)].

## VI. DISCUSSION

Two major questions arise from the experimental results shown in the previous sections:

- (i) What can explain the major difference between the polarization properties of SK and DE QDs?
- (ii) How can we explain such large DLPs in individual SK QDs?

$k \cdot p$  calculations performed in Sec. II show that the valence band mixing of DE QDs is slightly more sensitive to inplane shape anisotropy than SK QDs and that both SK and DE QDs behave very similarly regarding to stress anisotropy. The stark difference observed experimentally between the polarization properties of ZB and DE QDs thus evidences that the nucleation process leads to very different degree of inplane anisotropy. Since the SK growth mode is a strain-based process where the stress building up in a two-dimensional layer is released by formation of three-dimensional islands, the resulting quantum dot strongly depends on the local strain field of the epilayer on which it is grown. Similarly to bulk ZB GaN [23] and as the elongation of the AlN grains evidences, the local strain field has a favored orientation that commands the SK QD anisotropy.  $k \cdot p$  calculations [Fig. 1(c)] suggest that the large DLPs found in SK QDs cannot be explained by shape anisotropy alone. As a result, either QDs are submitted to large stress values ( $>2$  GPa) or both stress and shape anisotropy compound to lead to large valence band mixing amplitudes [see closed triangle in Fig. 1(c)]. On the opposite, the formation of DE QDs depends mainly on the formation of Ga droplets and its subsequent nitridation, which are barely

influenced by the local strain field. The shape of DE QDs is thus more symmetric and more randomly distributed than the shape of SK QDs. Regarding stress, although the AlN capping layer subjects DE QDs and SK QDs to a similar stress level, the average stress anisotropy in DE QDs and SK QDs differs because the nucleation site of SK QDs depends on the local strain field while the nucleation site of DE QDs is blind to it. As a result, DE QDs cover a larger range of DLP values that depend on whether or not the valence band mixing induced by the DE QD shape anisotropy compensates or compounds with the external stress [see  $k \cdot p$  calculations values indicated by triangles of Fig. 1(d)]. It is worth mentioning that it has been shown in other material systems that DE QDs can be elongated along one of the main crystallographic axes [28] due to anisotropic adatom migration or anisotropic surface tensions at the solid interface with the droplet. The lack of polarization of mesoscopic DE QD ensembles and the smaller DLP of single ZB GaN DE QDs show that such effects have a lower influence on the valence band mixing as compared to strain-based effects involved in the SK process.

Furthermore, we would like to mention that the present results on single SK QDs may shed new light on the previous report by Lagarde *et al.* regarding the macroscopic polarization properties of an 18-layer stack of SK ZB GaN QDs grown on 3C-SiC/Si (001) by plasma-assisted molecular beam epitaxy [7]. When measuring the macrophotoluminescence of the QD ensemble, Lagarde *et al.* observe a large DLP under a quasiresonant excitation linearly polarized along [110] and  $\bar{[110]}$  and a DLP close to 0 under quasiresonant excitations either circularly polarized or linearly polarized along [100] or  $[010]$ . Lagarde *et al.* subsequently claim that it indicates the absence of valence band mixing in ZB GaN QDs. However, single QDs studied in the current work are at odds with such a conclusion. Moreover, similar quasiresonant excitation results on a macroscopic scale may actually be obtained even with a large valence band mixing amplitude in individual QDs, providing that the average oscillator strengths of APD and  $\overline{\text{APD}}$  QD ensembles are equal. The present results would also explain why Lagarde *et al.* have not been able to observe a conversion from linearly polarized  $|X\rangle$  and  $|Y\rangle$  states to circularly polarized  $|\pm 1\rangle$  states when applying a [001]-oriented magnetic field up to 4T. It should, however, be noted that the structural properties of the QDs used in Ref. [7] may not be as dramatically impacted by APDs as the QDs studied in the present work, especially because stacking a large number of QDs can lead to a stress-mediated change of their structural properties.

Let us finish this discussion with a few remarks on relaxation mechanisms occurring in the investigated ZB GaN QDs. As mentioned in Sec. II and in the Appendix, under weak nonresonant excitation the optical anisotropy of the neutral excitons can only be observed if in addition to the radiative recombination from  $|\tilde{X}\rangle$  and  $|\tilde{Y}\rangle$  states, there exists another efficient relaxation mechanism such as nonradiative recombination, coupling to dark states or longitudinal exciton spin relaxation between bright excitons [8]. First, nonradiative recombinations are not likely to be efficient at low temperature and would rather become significant from 75 K according to additional nonresonant time-resolved  $\mu\text{PL}$  measurements on single QDs (not shown here). Second, the rate of relaxation to dark states could not be extracted from our time-resolved

$\mu\text{PL}$  data, but it has been shown to be negligible compared to  $\gamma_x$  and  $\gamma_y$  in CdSe/ZnS [29] and InAs/GaAs QDs [8] at low temperature. Third, regarding the longitudinal exciton spin relaxation between bright states, the literature on the topic is still unclear. On one hand, time-resolved PL measurements of an InAs/GaAs QD ensemble under resonant excitation by Paillard *et al.* [30] have shown that the QD exciton spin is frozen at low temperature but that longitudinal exciton spin relaxation becomes rapidly efficient with increasing temperature. With similar measurements on a ZB GaN/AlN QD ensemble, Lagarde *et al.* [7] conclude to an inefficient longitudinal exciton spin relaxation up to room temperature. On the other hand, nonresonant steady-state and time-resolved measurements on individual InAs/GaAs QDs by Favero *et al.* have shown that the DLP does not depend on temperature up to 70 K [31] and suggests that the QD exciton spin relaxation between bright states is efficient even at low temperature [8]. To get some insight into that matter, we perform additional temperature-dependent polarization measurements between  $T = 4$  K and  $T = 100$  K on three single DE QDs presenting DLPs lower than 1 (Fig. 6). In the case of a thermally activated relaxation process, one would expect the DLP to increase with temperature, up to its maximum value  $(\gamma_x - \gamma_y)/(\gamma_x + \gamma_y)$ . However, none of the DE QDs studied here exhibits such a behavior, remaining constant within the error up to 100 K. This suggests that the additional relaxation mechanism is already efficient at low temperature. This is similar to what has been observed by Favero *et al.* in InAs/GaAs QDs [8,31] but without information on the dark-state coupling rate and the exciton charge state, it is difficult to conclude whether or not the longitudinal exciton spin relaxation between bright states is allowed in the studied DE QDs: one would need to perform additional time-resolved measurements under resonant excitation to have a clear picture of the relaxation mechanism.

## VII. CONCLUSION

In summary, we have shown how the growth process of ZB GaN QDs influences their polarization properties. On one hand, we have shown that the orientation of antiphase domains determines the polarization orientation of SK QDs. Antiphase domains induce significant inplane anisotropy in the shape and strain distribution of individual QDs, which leads to a large valence band mixing. This valence band mixing is revealed by the very large DLPs observed in individual SK QDs. Such highly-polarized ZB GaN QDs have a high potential as triggered single-photon sources for quantum key distribution based on quantum polarization encoding [32] or other polarization-sensitive optoelectronics. From that perspective, SK ZB GaN QDs present significant advantages over their wurtzite counterparts since wurtzite GaN QDs exhibit DLPs ranging from 30% to 90% with no full linear polarization [33,34]. On the other hand, the DE process allows for the fabrication of QDs exhibiting a lower structural anisotropy. It leads to unpolarized DE QD ensembles that are insensitive to the presence of antiphase domains and to a lower valence band mixing in individual DE QDs. As a result, although single QDs presenting an isotropic inplane polarization have not been found yet, the DE technique seems to be more promising than the SK growth mode for the use of ZB GaN QDs in quantum devices based on entangled photon pairs.

## ACKNOWLEDGMENTS

The authors thank M. J. Holmes and E. Harbord for fruitful discussions. This work was supported by the Project for Developing Innovation Systems of the Ministry of Education, Culture, Sports, Science and Technology (MEXT), by Japan Society for the Promotion of Science (JSPS) through its “Funding Program for world-leading Innovation R&D on Science and Technology (FIRST Program), and by the DFG graduate program GRK 1464 “Micro- and Nanostructures in Optoelectronics and Photonics.”

APPENDIX:  $k \cdot p$  CALCULATIONS

ZB GaN/AlN QD  $k \cdot p$  calculations are carried out for the geometries exhibited in Fig. 7 using the Nextnano toolbox. Similar to Ref. [35], and in agreement with structural data [17,21], SK GaN QDs are modeled as truncated pyramids

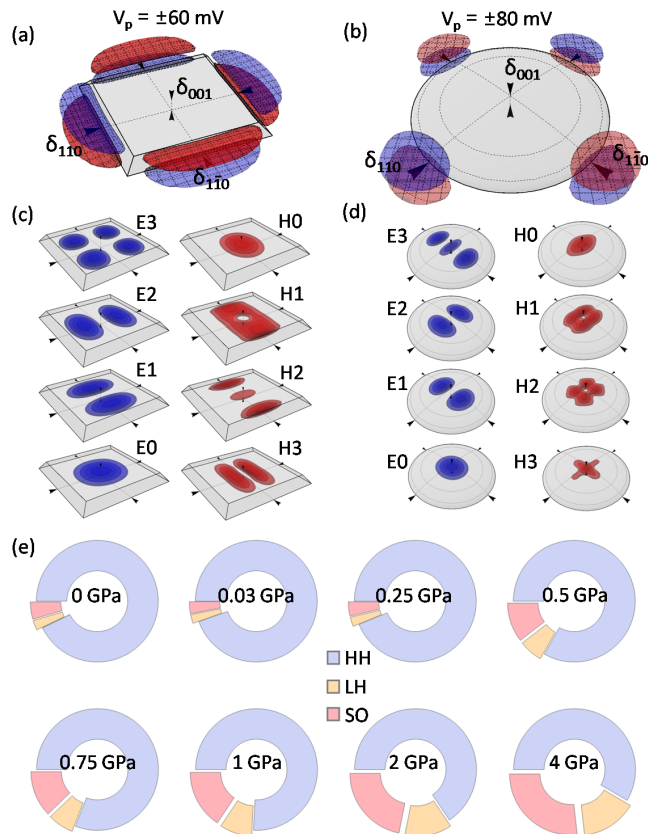


FIG. 7. (Color online) Isosurfaces of the piezoelectric potential (a)  $V_p = \pm 60$  mV for truncated pyramid SK QDs and (b)  $V_p = \pm 80$  mV for lens-shape DE QDs. (c) Isosurfaces of probability density  $|\langle \psi | \psi \rangle|^2$  for the first four electron and hole states as obtained from eight-band  $k \cdot p$  calculations of symmetric truncated pyramid SK QDs with  $\sigma = 0$ . The state energies are  $E_{E0} = 3.4621$  eV,  $E_{E1} = 3.4771$  eV,  $E_{E2} = 3.479$  eV,  $E_{E3} = 3.4937$  eV,  $E_{H0} = -0.1847$  eV,  $E_{H1} = -0.1875$  eV,  $E_{H2} = -0.1889$ , and  $E_{H3} = -0.1895$  eV. (d) Same as (c) for lens-shape DE QDs. The state energies are  $E_{E0} = 2.9561$  eV,  $E_{E1} = 2.9862$  eV,  $E_{E2} = 2.9960$  eV,  $E_{E3} = 3.0188$  eV,  $E_{H0} = -0.7329$  eV,  $E_{H1} = -0.7378$  eV,  $E_{H2} = -0.7392$ , and  $E_{H3} = -0.7394$  eV. (e) Contribution of HH, LH, and SO bands to the ground-hole state of lens-shape DE QDs for various  $\sigma$  applied along [110].

with {111} facets, a 0.5-nm-thick wetting layer, a height  $\delta_{001} = 2.5$  nm, and an out-of-plane aspect ratio  $\delta_{110}/\delta_{001} = 10$ . In agreement with known structural data on uncapped QDs [18,21,22], DE GaN QDs are modeled as lens-shape QDs with no facet, no wetting layer, a height  $\delta_{001} = 2.5$  nm and an out-of-plane aspect ratio  $\delta_{110}/\delta_{001} = 10$ . The influence of inplane aspect ratio on the polarization properties of GaN QDs is obtained by both eight-band and six-band  $k \cdot p$  calculations. The methods lead to very similar results due to the large bandgap of GaN and to the small subsequent coupling between the valence and conduction bands. The influence of external stress is obtained only by six-band  $k \cdot p$  calculations. The Hamiltonian  $H$  is solved taking into account strain and piezoelectric effects. Material parameters are extracted from [35–37] and displayed in Table I. It should be noted that the band structure of zinc-blende GaN and AlN is not fully known, so that a number of band structure parameters are extracted from theoretical works but are yet to be confirmed experimentally. In addition, parameters extracted from both experimental and theoretical works can be scattered, and an average value is thus used in the present calculations, following Ref. [36]. As a result, although similar parameters have been used in previous works focusing on ZB GaN QDs (see, e.g., Refs. [27,35]), we would like to stress that the present  $k \cdot p$  calculations have an interesting qualitative merit but can be quantitatively debatable.

As an example, the piezoelectric field and the probability densities of hole and electron states are exhibited in Fig. 7 for symmetric truncated pyramid SK QDs and lens-shape DE QDs with no externally applied stress. The ground-state exciton transition energies are, respectively, 3.60 and 3.65 eV. The polarization properties of the QDs are directly derived

TABLE I. List of the material parameters used in  $k \cdot p$  calculations. Values indicated by superscript a, b, c are, respectively, extracted from Refs. [35–37].

Parameters	GaN	AlN
Static dielectric constant $\epsilon_{\text{stat}}$	9.7 <sup>a</sup>	9.7 <sup>a</sup>
Optical dielectric constant $\epsilon_{\text{opt}}$	5.3 <sup>a</sup>	5.3 <sup>a</sup>
Lattice parameter $a$ (Å)	4.5 <sup>b</sup>	4.38 <sup>b</sup>
$\Gamma$ bandgap $E_g$ (eV)	3.299 <sup>b</sup>	5.4 <sup>b</sup>
Valence band offset (eV)	−0.7 <sup>b</sup>	−1.5 <sup>b</sup>
Spin-orbit split-off $\Delta_{SO}$ (meV)	17 <sup>b</sup>	19 <sup>b</sup>
$\Gamma$ effective mass $m_e$	0.15 <sup>b</sup>	0.25 <sup>b</sup>
HH effective mass $m_{hh}$	1.3 <sup>c</sup>	0.3
LH effective mass $m_{lh}$	0.19 <sup>c</sup>	0.3 <sup>c</sup>
SO effective mass $m_{so}$	0.29 <sup>b</sup>	0.47 <sup>b</sup>
Luttinger parameter $\gamma_1$	2.70 <sup>b</sup>	1.92 <sup>b</sup>
Luttinger parameter $\gamma_2$	0.76 <sup>b</sup>	0.47 <sup>b</sup>
Luttinger parameter $\gamma_3$	1.11 <sup>b</sup>	0.85 <sup>b</sup>
Kane energy $E_p$ (eV)	25 <sup>b</sup>	27.1 <sup>b</sup>
Kane parameter $F$	−0.95 <sup>b</sup>	−1.01 <sup>b</sup>
Conduction band deformation potential $a_c$ (eV)	−6.71 <sup>b</sup>	−4.5 <sup>b</sup>
Valence band deformation potential $a_v$ (eV)	−0.69 <sup>b</sup>	−4.9 <sup>b</sup>
Piezoelectric constant $e_{14}$ (C · m <sup>−2</sup> )	0.56	0.92
Elastic coefficient $c_{11}$ (GPa)	293 <sup>b</sup>	304 <sup>b</sup>
Elastic coefficient $c_{12}$ (GPa)	159 <sup>b</sup>	160 <sup>b</sup>
Elastic coefficient $c_{44}$ (GPa)	155 <sup>b</sup>	193 <sup>b</sup>

from the dipole matrix elements calculated between the hole and electron ground states for light propagating in the [001] direction and various inplane polarizations, following Ref. [35] for six-band  $k \cdot p$  and Ref. [38] for eight-band  $k \cdot p$ . We should note that in the case of single QDs observed under weak nonresonant excitation, the DLPs directly derived from dipole matrix elements can be experimentally observed only if radiative recombination rates  $\gamma_x$  and  $\gamma_y$  are much smaller than the rate of one additional relaxation channel [8], e.g., nonradiative recombination, coupling to dark states or longitudinal exciton spin relaxation between bright states. In such conditions the polarization measurements can

fully reveal the QD valence band mixing, leading to the maximum observable DLP  $(\gamma_x - \gamma_y)/(\gamma_x + \gamma_y)$ . This is the assumption we use when comparing our  $k \cdot p$  calculations to the experimental results, which agrees well with the large DLPs up to 100% observed in the present experiments and to the temperature-independent DLPs observed up to 100 K.

The contribution of HH, LH, and SO bands to the ground hole state of lens-shape DE QDs is displayed for various  $\sigma$  in Fig. 7(e). It highlights the fact that the DLP found in ZB GaN QDs is due to a mixing of the HH with both the LH and SO bands.

- 
- [1] S. Kako, C. Santori, K. Hoshino, S. Gotzinger, Y. Yamamoto, and Y. Arakawa, *Nat. Mater.* **5**, 887 (2006).
- [2] M. J. Holmes, K. Choi, S. Kako, M. Arita, and Y. Arakawa, *Nanoletters* **14**, 982 (2014).
- [3] J. Simon, N. T. Pelekanos, C. Adelman, E. Martinez-Guerrero, R. André, B. Daudin, L. S. Dang, and H. Mariette, *Phys. Rev. B* **68**, 035312 (2003).
- [4] J. P. Garayt, J. M. Gérard, F. Enjalbert, L. Ferlazzo, S. Founta, E. Martinez-Guerrero, F. Rol, D. Araujo, R. Cox, B. Daudin, B. Gayral, L. S. Dang, and H. Mariette, *Physica E* **26**, 203 (2005).
- [5] S. Sergent, S. Kako, M. Bürger, D. J. As, and Y. Arakawa, *Appl. Phys. Lett.* **103**, 151109 (2013).
- [6] S. Kako, M. Holmes, S. Sergent, M. Bürger, D. J. As, and Y. Arakawa, *Appl. Phys. Lett.* **104**, 011101 (2014).
- [7] D. Lagarde, A. Balocchi, H. Carrere, P. Renucci, T. Amand, and X. Marie, S. Founta, H. Mariette, *Phys. Rev. B* **77**, 041304(R) (2008).
- [8] I. Favero, G. Cassabo, C. Voisin, C. Delalande, Ph. Roussignol, R. Ferreira, C. Couteau, J. P. Poizat, and J. M. Gérard, *Phys. Rev. B* **71**, 233304 (2005).
- [9] Y. Léger, L. Besombes, L. Maingault, and H. Mariette, *Phys. Rev. B* **76**, 045331 (2007).
- [10] C. Tonin, R. Hostein, V. Voliotis, R. Grousson, A. Lemaitre, and A. Martinez, *Phys. Rev. B* **85**, 155303 (2012).
- [11] S. Ohno, S. Adachi, R. Kaji, S. Muto, and H. Sasakura, *Appl. Phys. Lett.* **98**, 161912 (2011).
- [12] E. Harbord, Y. Ota, Y. Igarashi, M. Shirane, N. Kumagai, S. Ohkouchi, S. Iwamoto, S. Yoro, and Y. Arakawa, *Jpn. J. Appl. Phys.* **52**, 125001 (2013).
- [13] D. Gammon, E. S. Snow, B. V. Shanabrook, D. S. Katzer, and D. Park, *Phys. Rev. Lett.* **76**, 3005 (1996).
- [14] M. Bayer, G. Ortner, O. Stern, A. Kuther, A. A. Gorbunov, A. Forchel, P. Hawrylak, S. Fafard, K. Hinzer, T. L. Reinecke, S. N. Walck, J. P. Reithmaier, F. Klopff, and F. Schäfer, *Phys. Rev. B* **65**, 195315 (2002).
- [15] R. Seguin, A. Schliwa, S. Rodt, K. Pötschke, U. W. Pohl, and D. Bimberg, *Phys. Rev. Lett.* **95**, 257402 (2005).
- [16] G. Juska, V. Dimastrodonato, L. O. Mereni, A. Gocalinska, and E. Pelucchi, *Nat. Photon.* **7**, 527 (2013).
- [17] E. Martinez-Guerrero, C. Adelman, F. Chabuel, J. Simon, N. T. Pelekanos, G. Mula, B. Daudin, G. Feuillet, and H. Mariette, *Appl. Phys. Lett.* **77**, 809 (2000).
- [18] T. Schupp, T. Meisch, B. Neuschl, M. Feneberg, K. Thonke, K. Lischka, and D. J. As, *J. Cryst. Growth* **312**, 3235 (2010).
- [19] M. Zielinski, *Phys. Rev. B* **88**, 155319 (2013).
- [20] A. Lundskog, C.-W. Hsu, K. F. Karlsson, S. Amloy, D. Nilsson, U. Forsberg, P. O. Holtz, and E. Janzen, *Light: Sci. Appl.* **3**, e139 (2013).
- [21] T. Schupp, T. Meisch, B. Neuschl, M. Feneberg, K. Thonke, K. Lischka, and D. J. As, *Phys. Stat. Sol. (c)* **8**, 1495 (2011).
- [22] T. Schupp, T. Meisch, B. Neuschl, M. Feneberg, K. Thonke, K. Lischka, and D. J. As, *J. Cryst. Growth* **323**, 286 (2011).
- [23] R. M. Kemper, T. Schupp, M. Häberlen, T. Niendorf, H. J. Maier, A. Dempewolf, F. Bertram, J. Christen, R. Kirste, A. Hoffmann, J. Lindner, and D. J. As, *J. Appl. Phys.* **110**, 123512 (2011).
- [24] H. Nagasawa, M. Abe, K. Yagi, T. Kawahara, and N. Hatta, *Phys. Stat. Sol. (b)* **245**, 1272 (2008).
- [25] S. Sergent, S. Kako, M. Bürger, T. Schupp, D. J. As, and Y. Arakawa, *Appl. Phys. Lett.* **105**, 141112 (2014).
- [26] C. Kindel, S. Kako, T. Kawano, H. Oishi, Y. Arakawa, G. Hönig, M. Winkelkemper, A. Schliwa, A. Hoffmann, and D. Bimberg, *Phys. Rev. B* **81**, 241309(R) (2010).
- [27] H. Tong and M. W. Wu, *Phys. Rev. B* **83**, 235323 (2011).
- [28] T. Mano, M. Abbarchi, T. Kuroda, C. A. Mastrandrea, A. Vinattieri, S. Sanguinetti, K. Sakoda, and, M. Gurioli, *Nanotechnology* **20**, 395601 (2009).
- [29] O. Labeau, P. Tamarat, and B. Lounis, *Phys. Rev. Lett.* **90**, 257404 (2003).
- [30] M. Paillard, X. Marie, P. Renucci, T. Amand, A. Jbeli, and J. M. Gérard, *Phys. Rev. Lett.* **86**, 1634 (2001).
- [31] I. Favero, G. Cassabo, A. Jankovic, R. Ferreira, D. Darson, C. Voisin, C. Delalande, Ph. Roussignol, A. Badolato, P. M. Petroff, and J. M. Gérard, *Appl. Phys. Lett.* **86**, 041904 (2005).
- [32] A. Muller, J. Breguet, and N. Gisin, *Europhys. Lett.* **23**, 383 (1993).
- [33] R. Bardoux, T. Guillet, B. Gil, P. Lefebvre, T. Bretagnon, T. Taliercio, S. Rousset, and F. Semond, *Phys. Rev. B* **77**, 235315 (2008).
- [34] S. Amloy, K. H. Yu, K. F. Karlsson, R. Farivar, T. G. Andersson, and P. O. Holtz, *Appl. Phys. Lett.* **99**, 251903 (2011).
- [35] V. A. Fonoberov and A. Balandin, *J. Appl. Phys.* **94**, 7178 (2003).
- [36] I. Vurgaftman and J. R. Meyer, *J. Appl. Phys.* **94**, 3675 (2003).
- [37] W. J. Fan, M. F. Li, and T. C. Chong, *J. Appl. Phys.* **79**, 188 (1996).
- [38] O. Stier, Ph.D. thesis, Technische Universität, Berlin, 2001.